Article

Power Mode Division Control Strategy for AC/DC Microgrids Considering SOC

Jiangzhou Cheng [1], Di Xiang [1,*], Cheng Fang [2] and Zhehao Hu [1]

[1] College of Electricity and New Energy, Three Gorges University Yichang, Yichang 443002, China; chengjiangzhou@ctgu.edu.cn (J.C.); 202208580121093@ctgu.edu.cn (Z.H.)
[2] State Grid Hubei Electric Power Company, Yichang Power Supply Company, Yichang 443000, China; m18371793297@163.com
[*] Correspondence: 202208580121255@ctgu.edu.cn

Abstract: Using hybrid energy storage systems, we propose a power mode partitioning control strategy for AC/DC microgrids that effectively mitigates frequency and voltage fluctuations. By incorporating composite virtual impedance, we categorize the state of charge (SOC) into five distinct operational modes. Supercapacitors, known for their dynamic response, are prioritized to counteract power fluctuations. We assign these operational modes to the AC and DC subnetworks based on real-time changes in frequency and voltage. When significant fluctuations occur, coordinated power transmission between the subnetworks and support from the energy storage system ensure that frequency and voltage remain within acceptable limits. Simulations conducted in MATLAB/Simulink confirmed that this control strategy stabilized power fluctuations and addressed the challenges of overcharging and overdischarging in storage batteries.

Keywords: AC and DC microgrids; state of charge; hierarchical coordination control; hybrid energy storage

1. Introduction

With the increasing adoption of distributed energy sources, their inherent volatility and intermittency pose significant challenges to the stability of the power grid [1]. Microgrids, particularly AC/DC microgrids that combine the benefits of both AC and DC systems along with distributed generation and energy storage, have emerged as promising solutions to these challenges. These microgrids are poised to play a critical role in addressing the complexities of new energy integration [2,3]. Currently, AC and DC microgrids are interconnected through converters, which leads to closely related power fluctuations between the two subnetworks [4].

Researchers worldwide have extensively studied power coordination control in AC/DC microgrids. Some [5,6] have proposed multimode coordinated control strategies that classify operational modes based on the state of charge (SOC) of energy storage systems, particularly under islanded conditions. However, these approaches often rely solely on droop control to maintain autonomy between the subnetworks, overlooking the need for power transmission in cases of power surplus or deficit. Others [7] have suggested dynamic power control strategies that consider bilateral inertia for interconnected converters, but these methods struggle to effectively suppress voltage and frequency fluctuations, especially under complex load conditions. Traditional filter-based strategies have also been explored for managing power distribution in the presence of distributed energy resources,

yet challenges such as underutilization of supercapacitor capacity and issues with battery overcharging or overdischarging persist [8,9].

Reference [10] introduces a centralized power allocation method that utilizes supercapacitors to mitigate instantaneous power fluctuations, but it overlooks power distribution within hybrid energy storage systems. This omission can lead to exceeding the state of charge (SOC) limits, compromising the system's to compensate effectively. Reference [11] explores the use of centralized filters and wavelet packet decomposition to adjust filter time constants for power distribution, but in scenarios requiring high accuracy in power signal acquisition, this approach may cause deviations in DC bus voltage, negatively impacting the dynamic stability of AC/DC microgrids. While Reference [12] applies a fuzzy algorithm to optimize the output power of hybrid energy storage based on supercapacitor SOC, it does not fully address frequency fluctuation issues in the AC subnetwork or the challenges of battery overcharging and overdischarging.

Reference [13] proposes two operational modes for AC/DC hybrid microgrids but struggles with the limitations of droop control in allocating hybrid energy storage power according to frequency variations, leading to insufficient load handling. In contrast, our proposed method not only further subdivided the coworking modes of microgrids but introduced virtual impedance to improve the power distribution capability of hybrid energy storage systems. The load capacity of our proposed method is larger, which is more conducive to the stabilization of the microgrid.

Reference [14] achieves the delay of hybrid energy storage overrun by adaptive virtual inertia control for DC microgrid. However, compared with our approach, this literature still adopts sag control for hybrid energy storage and suffers from the problem that the response time is too slow to accurately determine the state of hybrid energy storage, which is prone to cause overcharging and overdischarging of batteries and supercapacitors in hybrid energy storage.

To overcome these challenges, this paper proposes a power mode division control strategy for AC/DC microgrids. Our approach aims to prevent overcharging and overdischarging of the energy storage system while effectively suppressing power fluctuations in microgrids with high-power load access. By accurately dividing the working modes of the AC/DC microgrid and the energy storage system, our strategy enhances the stability of determining the operating status of AC/DC subnetworks. Compared to other control methods, our proposed strategy significantly improves the dynamic stability of the microgrid when connected to high-power loads and exhibits a stronger capacity to smooth out load fluctuations. The effectiveness of this power mode division control strategy is validated through simulations using MATLAB/Simulink.

2. AC/DC Microgrid Topology

The AC/DC microgrid consists of an AC subnetwork, a DC subnetwork, and interconnected converters (ICs). The AC subnetwork includes the point of common coupling (PCC), which manages transitions between grid-connected and islanded states, wind turbines, and AC loads. Wind turbines connect to the AC bus through a machine-side AC/DC converter and a grid-side DC/AC converter. The DC subnetwork features distributed photovoltaic (DP) systems, hybrid energy storage systems (HESS), and DC loads [14]. The DP system operates in maximum power point tracking (MPPT) mode [15] while the HESS connects to the DC bus via a bidirectional DC–DC converter, providing crucial energy support to maintain system stability during islanded operation. ICs link the AC and DC subnetworks, enabling power transfer and mutual support. Figure 1 illustrates the topology of the AC/DC hybrid microgrid discussed in this paper.
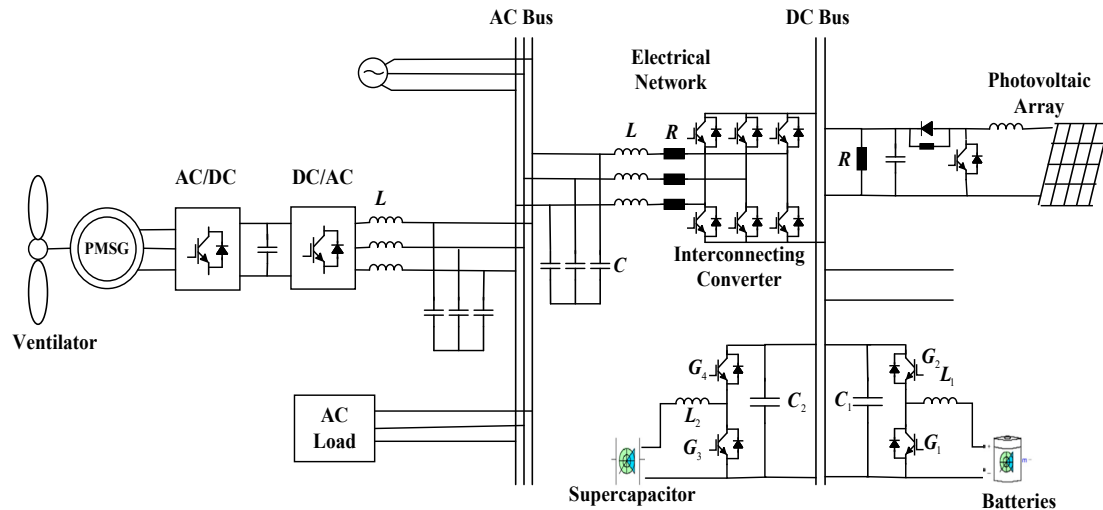
Figure 1. AC/DC microgrid topology.

3. Control Methods for AC/DC Microgrids

3.1. Interconnected Converter Control

In controlling the interconnected converters (ICs) within the AC/DC microgrid, we used a virtual synchronous generator (VSG) adaptive control approach. This method models the VSG based on a classic second-order model of a synchronous generator. The primary frequency regulation of the simulated synchronous generator is controlled by one parameter, while another parameter handles the excitation regulation. The relationships governing these controls are expressed mathematically as follows:

$$P_{\mathrm{m}} = P_{\mathrm{ref}} - K_1(\omega - \omega_{\mathrm{ref}}) \tag{1}$$

Equation (1) shows the reference value of active power, denoted as P_{ref}, and the frequency modulation (FM) coefficient, represented as K_1.

$$E = (U_{\mathrm{dc.n}} - U_{\mathrm{dc}})K_2 + (Q_{\mathrm{ref}} - Q)K_3 \tag{2}$$

Equation (2) describes the relationship between electromotive force (EMF) and the actual and reference voltage values during system operation. The system's actual voltage value is denoted by U_{dc} while $U_{\mathrm{dc.n}}$ represents the reference voltage. The equation also incorporates the voltage regulation coefficient K_4 and the reactive voltage sag coefficient K_3.

Additionally, Q_{ref} and Q represent the reference and actual values of reactive power, respectively.

$$\Delta P_{\mathrm{dc}} = K_4(U_{\mathrm{dc.n}} - U_{\mathrm{dc}}) + CU_{\mathrm{dc.n}}\frac{dU_{\mathrm{dc}}}{dt} \tag{3}$$

Equation (3) presents the control expression for the virtual synchronous generator (VSG). This equation is crucial for regulating the system's voltage and reactive power, ensuring that the VSG adapts to changes in the microgrid's operating conditions to maintain stability and performance.

Equation (3) defines the active power variation (ΔP_{dc}), the DC-side sag factor (K_4), and the DC-side capacitance (C). These factors influence how the system responds to changes in power demand or supply, helping to stabilize the DC bus voltage.

The power exchange between the AC and DC subnetworks takes place through the interconnected converters when there is an imbalance in power supply and demand. The direction of power flow is considered positive when moving towards the inverter. Equation (4) provides the expression for power transmission through the interconnected converter,

which governs how power is transferred between the AC and DC subnetworks to maintain system stability.

$$P_{\text{IC}} = (K_{\text{P}} + \frac{K_{\text{i}}}{s})(f_{\text{s}} - U_{\text{dc.s}}) \tag{4}$$

The proportional and integral coefficients, denoted as K_{p} and K_{i}, are key parameters of the PI controller. By adjusting these coefficients, the system ensures that the control objectives are met, maintaining stability and desired performance levels.

3.2. Hybrid Energy Storage System Control and State Division

In controlling the hybrid energy storage system (HESS), which includes both batteries and supercapacitors, power is transferred between the AC/DC microgrid and the HESS through interconnected converters (ICs). This transfer stabilizes the AC frequency and the DC bus voltage [16]. The introduction of virtual resistance and virtual capacitance into the HESS allows us to express the relationship among the currents of the battery, supercapacitor, and equivalent load, as shown in Equation (5). This approach enhances the system's ability to manage power fluctuations and maintain overall grid stability.

$$\begin{cases} I_1 = \frac{1}{R_v C_v s + 1} I \\ I_2 = \frac{R_v C_v s}{R_v C_v s + 1} I \end{cases} \tag{5}$$

In this context, I_1 represents the battery output current, I_2 is the output current of the supercapacitor, R_v denotes the virtual resistance, and C_v stands for the virtual capacitance. The equivalent load current is denoted by I_{L}, while S is the frequency domain coefficient of the transfer function.

The current transfer functions for both the battery and supercapacitor are defined in Equation (6). These functions describe how the currents in the battery and supercapacitor respond to changes in the system, allowing for effective management of power distribution within the hybrid energy storage system.

$$\begin{cases} G_1 = \frac{1}{R_v C_v s + 1} \\ G_2 = \frac{R_v C_v s}{R_v C_v s + 1} \end{cases} \tag{6}$$

The battery's current transfer function acts like a low-pass filter, while the supercapacitor's current transfer function behaves like a high-pass filter. Figure 2 illustrates the control strategy diagram for the hybrid energy storage system, showcasing how these components interact.
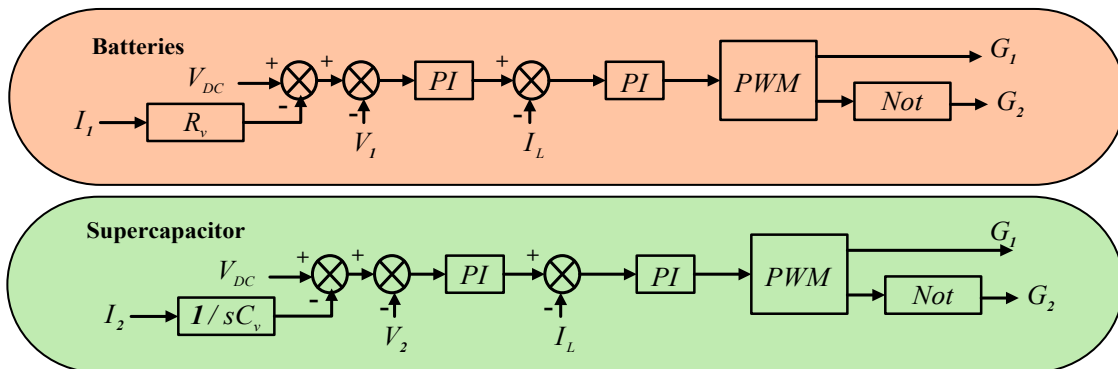

Figure 2. Block diagram of the control strategy for the energy storage system.

To maximize the rapid response capabilities of supercapacitors, the system classifies operating modes based on the state of charge (SOC) of both supercapacitors and batteries. As shown in Figure 3.
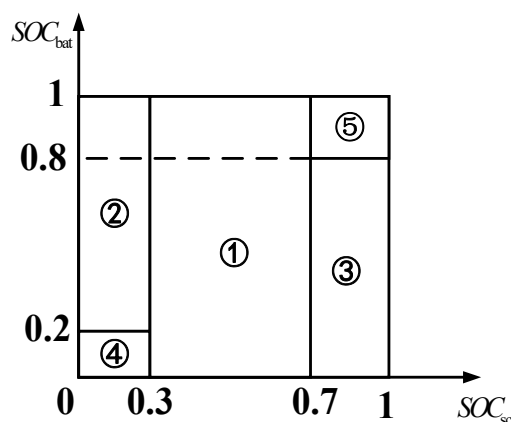

Figure 3. Segmentation of energy storage system operation modes.

Table 1 outlines the criteria for classifying and determining the operating states of the system, ensuring efficient power management and stability.

Table 1. Energy storage system operation states and the conditions of their activation.

Corresponding Area	Operational State	Condition of Judgment
①	Ultracapacitor charge and discharge; battery standby	$0.3 < SOC_{sc} < 0.7$
②	Supercapacitor charging; battery discharging	$\begin{cases} 0 < SOC_{sc} < 0.3 \\ 0.2 < SOC_{bat} < 1 \end{cases}$
③	Ultracapacitor discharge; battery charging	$\begin{cases} 0.7 < SOC_{sc} < 1 \\ 0 < SOC_{bat} < 0.8 \end{cases}$
④	Overdischarge protection	$\begin{cases} 0 < SOC_{sc} < 0.3 \\ 0 < SOC_{bat} < 0.2 \end{cases}$
⑤	Overcharge protection	$\begin{cases} 0.7 < SOC_{sc} < 1 \\ 0.8 < SOC_{bat} < 1 \end{cases}$

When the energy storage system enters the overdischarge protection state, corresponding to region ④, and both the AC and DC subnetworks have surplus power, the supercapacitors, with their high dynamic response, absorb the excess power from the microgrid. However, if both subnetworks are experiencing a power deficit and require support from the hybrid energy storage system, the system halts its operation to avoid further discharging, protecting the system from overdischarge.

Similarly, in the overcharge protection state, the hybrid energy storage system (HESS) stops absorbing surplus power from the AC/DC microgrid to prevent overcharging. This precautionary measure helps extend the lifespan of the batteries by ensuring they are not overcharged.

## 4. Power Coordination Control Strategy for AC/DC Microgrids Using Hybrid Energy Storage

4.1. Power Control Mode Division in AC/DC Microgrids

Interconnected converters link the AC and DC subnetworks, controlling the direction of power transmission based on changes in AC bus frequency and DC bus voltage. This control strategy significantly enhances the stability of the AC/DC microgrid. By normalizing the AC bus frequency and DC bus voltage, we can use consistent physical quantities to represent power flow between the subnetworks. Equation (7) illustrates this relationship.

$$\begin{cases} f_{s} = \frac{f - 0.5(f_{max} + f_{min})}{0.5(f_{max} - f_{min})} \\ U_{dc.s} = \frac{U_{dc} - 0.5(U_{dcmax} + U_{dcmin})}{0.5(U_{dcmax} - U_{dcmin})} \end{cases} \tag{7}$$

After normalization, the scalar values of AC frequency and DC bus voltage, denoted as f_s and $U_{dc.s}$, respectively, are both in the range $[-1, 1]$.

As illustrated in Figure 4, the operation states of the AC/DC microgrid are categorized based on the values of f_s and $U_{dc.s}$, as well as their ratios to constants a and b. This classification distinguishes between autonomous power operation modes and mutual assistance power operation modes [12]. The mutual assistance modes are further divided into three specific operational modes, each tailored to different conditions.
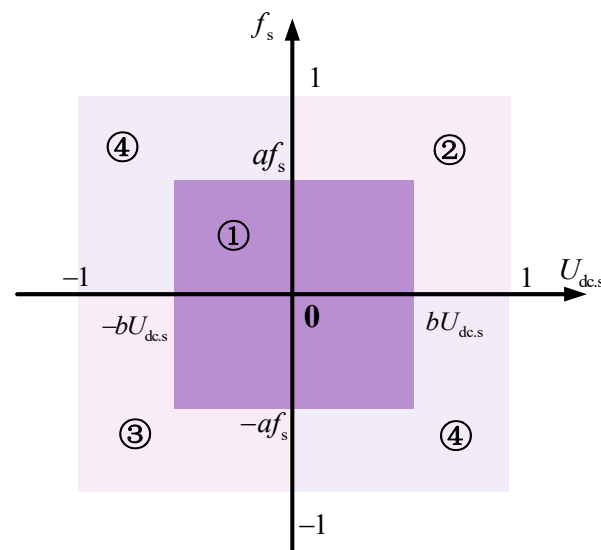
Figure 4. Classification of microgrid operation states.

When minor fluctuations arise, the AC/DC subnetworks can independently maintain stable operation, corresponding to region ① in Figure 4 During this period, the interconnected converters and energy storage systems remain in standby mode. Equation (8) outlines the criteria for determining the autonomous power mode.

$$\begin{cases} -af_{s} < f_{s} < af_{s} \\ -bU_{dc.s} < U_{dc.s} < bU_{dc.s} \end{cases} \tag{8}$$

In this equation, a represents the ratio of AC subnetwork frequency fluctuations to the permissible fluctuation range, while b denotes the ratio of DC bus voltage fluctuations to the allowed fluctuation range.

When AC frequency and DC bus voltage variations exceed the limits of region ①, the autonomous power mode is no longer sufficient to maintain stable power support for the

AC/DC microgrid. To prevent instability, the system shifts to mutual assistance power operation mode, where the hybrid energy storage system (HESS) takes an active role in coordinating power between the AC and DC subnetworks.

Region ② in Figure 4 represents the condition where both the AC and DC subnetworks have surplus power. Equation (9) outlines the criteria for identifying this state.

$$\begin{cases} 0 < f_\text{s} < 1 \\ bU_\text{dc.s} < U_\text{dc.s} < 1 \end{cases} \cup \begin{cases} af_\text{s} < f_\text{s} < 1 \\ 0 < U_\text{dc.s} < bU_\text{dc.s} \end{cases} \tag{9}$$

In region ③ of Figure 4, both the AC and DC subnetworks experience a power deficit. This condition arises under the criteria outlined in Equation (10).

$$\begin{cases} -1 < f_\text{s} < 0 \\ -1 < U_\text{dc.s} < -bU_\text{dc.s} \end{cases} \cup \begin{cases} -1 < f_\text{s} < -af_\text{s} \\ -bU_\text{dc.s} < U_\text{dc.s} < 0 \end{cases} \tag{10}$$

Region ④ of Figure 4 represents the scenario where either the AC subnetwork has a power surplus while the DC subnetwork faces a deficit, or the opposite occurs. Equation (11) defines the criteria for this state.

$$\begin{cases} f_\text{s}U_\text{dc.s} < 0 \\ 0 < |f_\text{s}| < 1 \\ bU_\text{dc.s} < |U_\text{dc.s}| < 1 \end{cases} \cup \begin{cases} f_\text{s}U_\text{dc.s} < 0 \\ af_\text{s} < |f_\text{s}| < 1 \\ 0 < |U_\text{dc.s}| < bU_\text{dc.s} \end{cases} \tag{11}$$

4.2. Division of Power Control Modes for Hybrid Energy Storage Systems

By examining the various working modes and power flows of hybrid energy storage systems within AC/DC microgrids, we can categorize the systems into five distinct modes. These modes are defined by the power surpluses and deficits of the AC and DC subgrids, represented by specific variables.

(1)　Mode 1: Supercapacitor Charging/Discharging, Battery on Standby

Mode 1 occurs when the DC subnetwork has a power surplus and the AC subnetwork faces a deficit. In this situation, the hybrid energy storage system (HESS) prioritizes the use of supercapacitors for charging or discharging, while the battery remains on standby, as outlined in Table 2.

Table 2. Hybrid energy storage system mode 1.

Working Condition	Condition of Judgment	HESS Operation
1	$P_\text{IC} < 0$	Supercapacitors absorb surplus power from AC and DC subgrids
2	$P_\text{IC} > 0$	Supercapacitors to support AC/DC subgrid shortage power
3	$P_\text{IC} < 0 \ \Delta P_\text{AC}^+ > \Delta P_\text{DC}^-$	Supercapacitor absorbs part of the surplus power on the AC side
	$P_\text{IC} > 0 \ \Delta P_\text{AC}^+ < \Delta P_\text{DC}^-$	Ultracapacitors support part of the missing power on the DC side

In the scenario where the DC subnetwork has a surplus of power while the AC subnetwork experiences a deficit, the hybrid energy storage system (HESS) still prioritizes the response from the supercapacitors.

(2)　Mode 2: Supercapacitors Charging, Batteries Discharging

In this mode, when the system is in mutual assistance power mode a, the supercapacitors absorb surplus power from the AC and DC subnetworks. In mutual assistance power mode b, corresponding to condition 4, the batteries supply power to cover the microgrid's deficit. When operating in mutual assistance power mode c, the HESS prioritizes the response for the supercapacitors.

(3)   Mode 3: Supercapacitors Discharging, Batteries Charging

When the system is in mutual assistance power mode a, corresponding to condition 5, the batteries supply the necessary power to the AC/DC subnetworks facing a deficit. In mutual assistance power mode b, the superconductors provide the needed power to cover the microgrid's deficit. In mutual assistance power mode c, similar to condition 3, the HESS prioritizes the supercapacitors' response.

(4)   Mode 4: HESS Overdischarge Protection

In mutual assistance power mode a, the system directs surplus power from the AC and DC subnetworks to the supercapacitors. When operating in mutual assistance power mode b, corresponding to condition 6, the system maintains the stability of the AC/DC microgrid by shedding load. In mutual assistance power mode c, the HESS either prioritizes the response of the supercapacitors or initiates load shedding to protect against overdischarge.

(5)   Mode 5: HESS Overcharge Protection

Under mutual assistance power mode a, corresponding to condition 7, the AC/DC microgrid increases load to maintain stability. In mutual assistance power mode b, the supercapacitors supply the necessary power to cover any deficit in the AC/DC subnetworks. In power mode c, the HESS either prioritizes the supercapacitors' response or increases the load on the AC/DC microgrid to prevent overcharging.

5. Simulation Verification

To validate the feasibility of the proposed SOC-based power coordination control strategy for AC/DC microgrids, a simulation model was developed using MATLAB/Simulink. The main parameters used in the simulation are listed in Table 3.

Table 3. Simulation parameters.

AC Subnetworks		DC Subnetworks	
$f_{\mathrm{max}}/\mathrm{Hz}$	50.5	$U_{\mathrm{dc.max}}/\mathrm{V}$	770
$f_{\mathrm{min}}/\mathrm{Hz}$	49.5	$U_{\mathrm{dc.min}}/\mathrm{V}$	730
P_L/kW	15	P_L/kW	12
$L_{\mathrm{f}}/\mathrm{mH}$	1.5	$L_{\mathrm{f}}/\mathrm{mH}$	0.8
$C_{\mathrm{f}}/\mu\mathrm{F}$	5000	$C_{\mathrm{f}}/\mu\mathrm{F}$	2500
a	0.4	b	0.4
HESS			
$S_{\mathrm{sc}}/\mathrm{F}$	100	$S_{\mathrm{Bat}}/(\mathrm{A.H})$	250
$U_{\mathrm{SC}}/\mathrm{V}$	220	$U_{\mathrm{Bat}}/\mathrm{V}$	400
$L_{\mathrm{sc}}/\mathrm{mH}$	0.5	L_{bat}/mH	0.5
Interconnecting Converter			
$L_{\mathrm{f.dc}}/\mathrm{mH}$	5	$C_{\mathrm{f.dc}}/\mu\mathrm{F}$	2500
$C_{\mathrm{dc}}/\mu\mathrm{F}$	5000	$L_{\mathrm{f.ac}}/\mathrm{mH}$	5
U_{dc}/V	750	$C_{\mathrm{f.ac}}/\mu\mathrm{F}$	250

5.1. Mode 1 Simulation Verification

The initial state of charge for both the batteries and supercapacitors was set to 0.5. Figure 5 depicts the simulation results based on the load variations of mode 1, detailed in Appendix A. In this setup, power transfer from the AC subnetwork to the DC subnetwork is considered positive. During the first second, the AC/DC microgrid operated in power autonomy mode, handling rated power loads with both the IC and HESS on standby. At the 1 s mark, the AC load decreased to 12 kW, causing the value of f_{s} to rise to 0.2 pu. Since this change did not exceed the threshold for switching operation modes, the microgrid remained in the same mode. However, after 2 s, it dropped to -0.6 pu because of increased load between the DC subgrids, surpassing the threshold and prompting the IC to transmit 6 kW

of power while the HESS supplied 1.8 kW to the AC subgrids from the supercapacitors. By 3 s, as the AC subnetwork load increased further, f_s decreased to −0.85 pu, leading the IC to transport −5 kW of power and the HESS to provide 8.4 kW to the AC subnetwork. At 4 s, distributed power was added on the DC side, stabilizing the AC subnetwork frequency and DC subnetwork voltage, with the battery remaining on standby throughout the process.
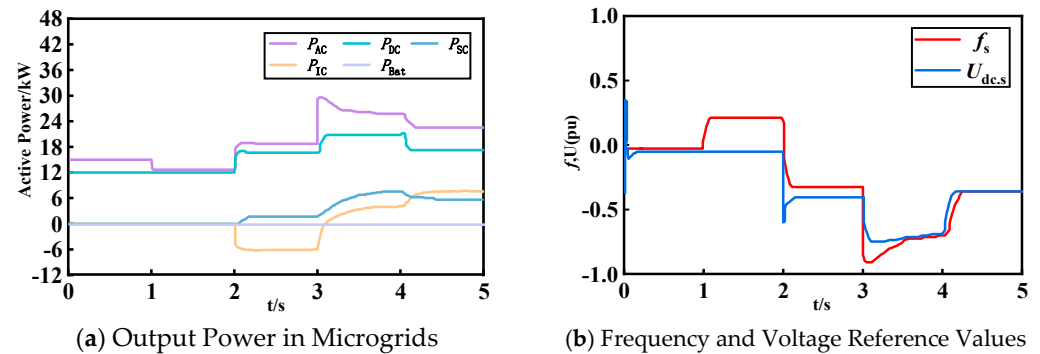

(**a**) Output Power in Microgrids (**b**) Frequency and Voltage Reference Values

Figure 5. Mode 1 simulation verification.

Figure 6 presents the simulation results using a traditional HESS control strategy under varying AC/DC loads between 2 and 4 s. At 2 s, with the AC load at 17 kW and the DC load at 15 kW, the HESS supported the AC/DC microgrid by initially outputting 1.5 kW from the supercapacitors, which then stopped operating after 0.1 s, leaving the batteries to continue providing 3.4 kW. By 3 s, as the AC subnetwork load increased further, the HESS continued to supply power, with the supercapacitors outputting 2 kW and the batteries delivering 11.5 kW. Compared with the mode 1 simulation using the hierarchical coordinated control method proposed in this study, it is clear that this approach significantly improved the utilization of supercapacitors while preventing overcharging and overdischarging of the batteries.
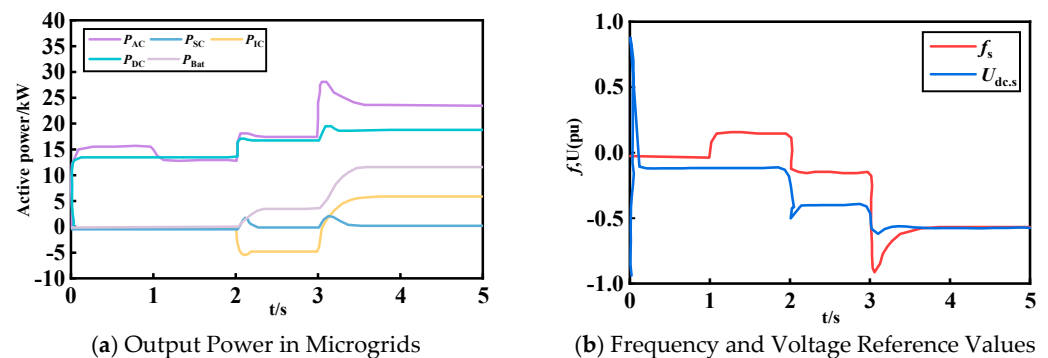

(**a**) Output Power in Microgrids (**b**) Frequency and Voltage Reference Values

Figure 6. Simulation verification of conventional HESS control strategy.

Conventional control methods have higher peaks in the frequency and voltage specification, and the battery is continuously discharged in conventional control methods, which is not conducive to the battery's cell life. The method we used determines that the battery is inactive at this time by determining the operating mode in which the microgrid is operating, and the power is delivered from the power surplus subgrid to the power deficit subgrid, while the supercapacitor also assumes a portion of the power support.

5.2. Mode 2 Simulation Verification

For the mode 2 simulation, the initial states of charge for the supercapacitor and battery were set to 0.25 and 0.5, respectively. The results, shown in Figure 7, indicate

that from 0 to 2 s, both the AC and DC subgrids experienced a power deficit, with f_s and $U_{dc.s}$ both at -0.5 pu. During this period, the AC/DC microgrid operated in power mutualization mode *b*, with the IC transmitting -1.68 kW and the HESS outputting 9 kW from the battery while the supercapacitor remained on standby. After 2 s, as the loads on the AC and DC subgrids decreased to 6 kW and 13 kW, respectively, f_s rose to 0.03 pu and $U_{dc.s}$ fell to -0.11 pu, causing the microgrid to shift into power autonomy mode. In this mode, power was redirected from the batteries to charge the supercapacitors, and the ICs stopped transmitting power.

(**a**) Output Power in Microgrids   (**b**) Frequency and Voltage Reference Values
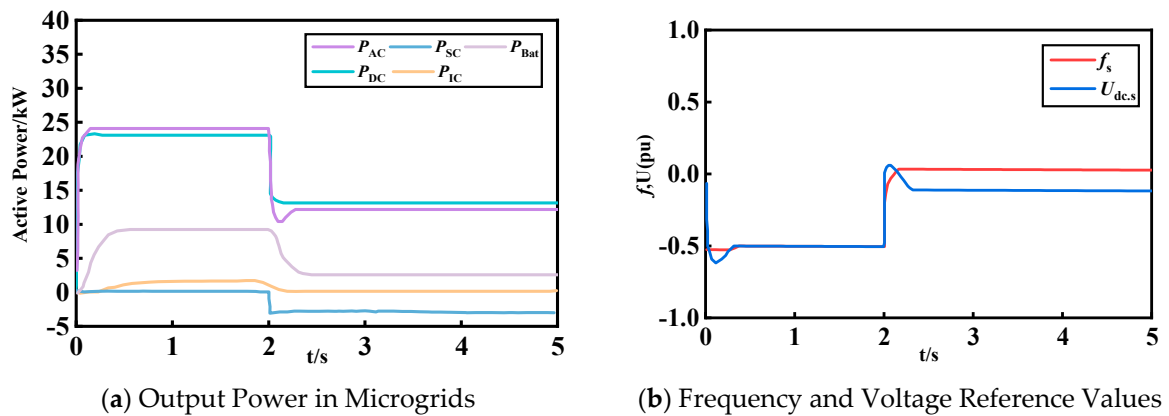
Figure 7. Mode 2 simulation verification.

5.3. Mode 3 Simulation Verification

The initial states of charge for the supercapacitors and batteries were set to 0.8 and 0.5, respectively. The simulation results for mode 3 are shown in Figure 8. From 0 to 2 s, neither HESS nor IC was needed to transfer power between the AC and DC subnetworks, as both the batteries and supercapacitors were well charged and storing energy. At 2 s, as the load decreased, the AC/DC subnetworks entered mutual assistance power mode a. In this mode, the batteries in the HESS absorbed 6 kW surplus power, while the supercapacitors remained on standby. After stabilization, f_s reached 0.4 pu and $U_{dc.s}$ reached 0.35 pu.

(**a**) Output Power in Microgrids   (**b**) Frequency and Voltage Reference Values
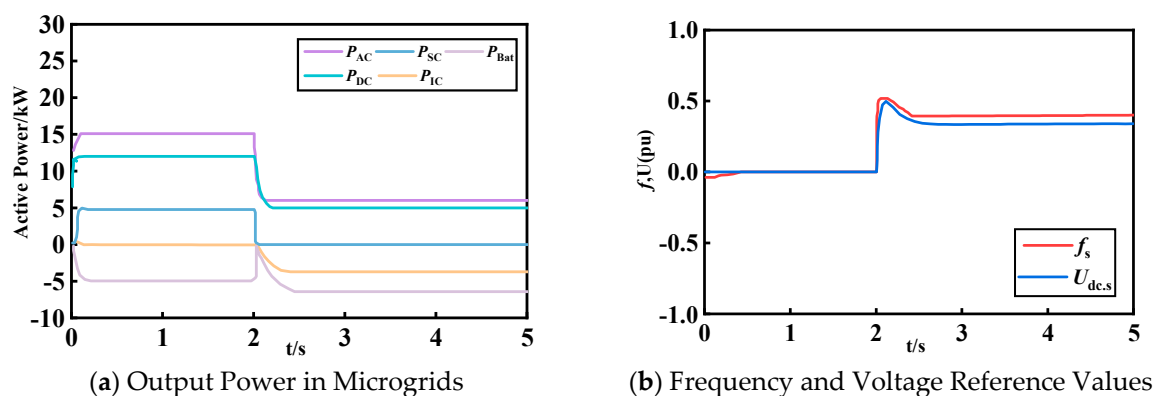
Figure 8. Mode 3 simulation verification.

5.4. Mode 4 Simulation Verification

The initial states of charge for the supercapacitors and batteries were set to 0.27 and 0.15, respectively. The simulation results for mode 4 are presented in Figure 9. From 0 to 2 s, both the AC and DC subnetworks were in a surplus power state, requiring the HESS to absorb the excess power. During this period, the AC/DC microgrid operated in mutual assistance power mode a, with the IC transmitting 4.2 kW of power, which was absorbed

by the supercapacitors. At 2 s, the AC/DC subnetwork experienced a load increase that exceeded the rated power capacity, resulting in a power deficit. The system then shifted to power mutualization mode b, with the IC transmitting 3.1 kW and the HESS activating overdischarge protection, which halted its operation. At 3 s, to prevent instability caused by excessive deviations in AC frequency and DC bus voltage, 4 kW and 9 kW loads were disconnected from the AC and DC subnetworks, respectively.
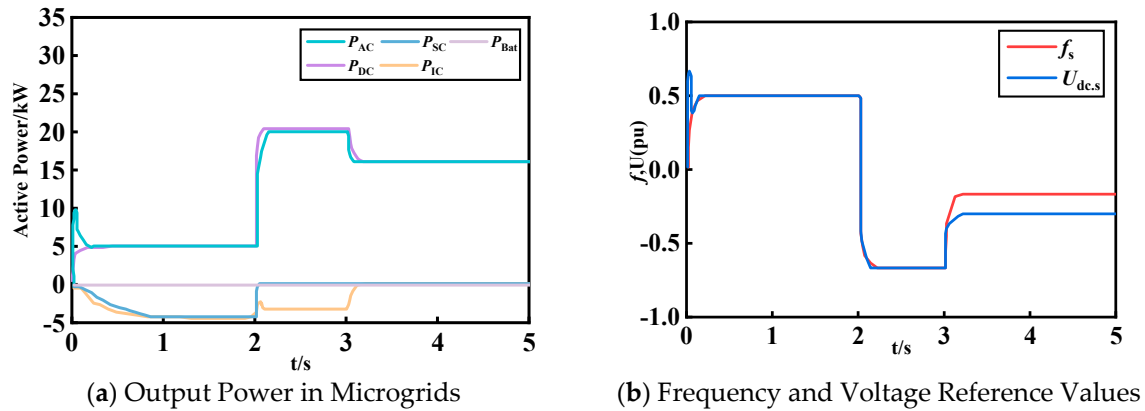

(**a**) Output Power in Microgrids (**b**) Frequency and Voltage Reference Values

Figure 9. Mode 4 simulation verification.

5.5. Mode 5 Simulation Verification

The initial states of charge for both the supercapacitor and the battery were set to 0.8. The simulation results for mode 5, as shown in Figure 10, indicate that at 0 to 2 s, both the AC and DC subnetwork loads exceeded their rated capacity. During this period, the AC/DC microgrid operated in mutual assistance power mode b, where the supercapacitors in HESS output 6.2 kW and the IC transmitted -0.46 kW of power between the AC and DC subnetworks. At 2 s, as the load on the AC and DC subnetworks decreased, the HESS entered overcharge protection mode and stopped operating. By 3 s, to prevent excessive deviations in key indicators that could lead to system instability, adjustable loads of 6 kW and 5.1 kW were added to the AC and DC subnetworks, respectively. At this point, f_s was 0.16 pu and $U_{dc.s}$ was 0.2 pu, allowing the AC/DC microgrid to function in power autonomy mode.
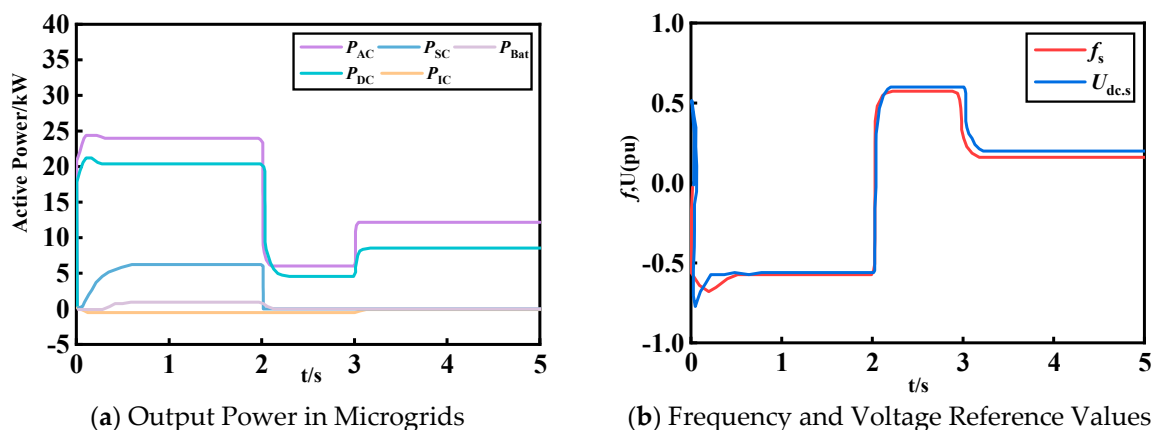

(**a**) Output Power in Microgrids (**b**) Frequency and Voltage Reference Values

Figure 10. Mode 5 simulation verification.

6. Conclusions

This paper presents a power mode division and control strategy for AC/DC microgrids that takes into account the state of charge (SOC) of the hybrid energy storage system (HESS). The following conclusions have been drawn from the study:

Unlike traditional energy storage system control strategies, this paper introduces composite virtual impedance into the HESS, allowing for the decomposition of energy storage power across high and low frequencies. This approach enables autonomous power allocation. By prioritizing the use of supercapacitors, which have a dynamic response capability, the system effectively mitigates power fluctuations caused by load variations between AC and DC subnetworks, thereby preventing overcharging and overdischarging of both batteries and supercapacitors.

At the same time, the study classifies the operating states of AC and DC microgrids using f_s and $U_{dc.s}$, proposing two modes: power autonomy mode and power mutualization mode. These modes facilitate power transfer between the two subgrids through IC coordination, ensuring balanced and efficient energy distribution.

The simulation results indicated that the proposed control strategy outperformed existing energy storage system controls by keeping AC frequency and DC bus voltage deviations within specified limits, even when high-power loads and distributed energy resources were integrated. This strategy effectively ensures the stability of AC/DC hybrid microgrid operations.

In the case of extreme loads, advanced load forecasting links can also be added to the energy management system, such as a short-term power load forecasting model based on complementary ensemble empirical modal decomposition (CEEMD) combined with the wavelet threshold method and a convolutional neural network (CNN), to improve the accuracy of load forecasting in order to make preparations for response in advance. At the same time, through power carrier wave and other communication means, power dispatching instructions are sent to users to guide them to reduce nonessential power consumption during peak load hours or increase power consumption during low load hours, so as to realize the balance of load. These are all directions that need more research in the future.

In the future, hydrogen energy, which is one of the main clean energy sources, should be considered to be introduced into the hybrid energy storage system, and the effect on the microgrid system, as well as the economic benefits of adopting hydrogen energy, should be studied.

Author Contributions: J.C.: data analysis, paper writing, investigation. D.X.: restructuring of paper, article idea, visualization. C.F.: data curation, investigation. Z.H.: methodology, article idea, analysis of results. All authors reviewed the manuscript. All authors have read and agreed to the published version of the manuscript.

Appendix A

Table A1. Load fluctuations in AC and DC microgrids.

Times/s		0~1	1~2	2~3	3~4	4~5
Mode 1	ACP_L/kW	15	12	12	23	23
	DCP_L/kW	12	12	22.5	18	18
Mode 2	ACP_L/kW	24	24	6	12	12
	DCP_L/kW	23	23	13	13	13
Mode 3	ACP_L/kW	15	15	6	6	6
	DCP_L/kW	12	12	5	5	5
Mode 4	ACP_L/kW	4.5	4.5	20	16	16
	DCP_L/kW	5	5	23	14	14
Mode 5	ACP_L/kW	24	24	6	12	12
	DCP_L/kW	20	20	4.5	8.1	8.1

References

1. Hassan, Q.; Hsu, C.Y.; Mounich, K.; Algburi, S.; Jaszczur, M.; Telba, A.A.; Viktor, P.; Awwad, E.M.; Ahsan, M.; Ali, B.M.; et al. Enhancing smart grid integrated renewable distributed generation capacities: Implications for sustainable energy transformation. *Sustain. Energy Technol. Assess.* **2024**, *66*, 103793. [CrossRef]

2. Nejabatkhah, F.; Li, Y.W. Overview of power management strate-gies of hybrid AC/DC microgrid. *IEEE Trans. Power Electron.* **2015**, *30*, 7072–7089. [CrossRef]

3. Liu, L.F.; Han, X.Q.; Ren, C.G. Multi-mode Operation Control Scheme for AC/DC Interfacing Converter Under Unbalanced Conditions in Hybrid Microgrid. *High Volage Eng.* **2019**, *45*, 4003–4012.

4. Jia, L.H.; Zhu, Y.Q.; Du, S.F. Control Strategy of Interlinked Converter for AC/DC Microgrid. *Autom. Electr. Power Syst.* **2016**, *40*, 98–104.

5. Ling, P.Y.; Mi, Y.; Li, H.P.; Jiang, E.Y.; Shi, S. Multi-mode Coordinated Control Strategy for AC/DC Hybrid Microgrid. *Electr. Power Constr.* **2022**, *43*, 77–86.

6. Kuang, H.H.; Tao, C.; Su, F.Q.; Kuang, W. A Control Strategy for lslanded AC/DC Hybrid Microgrid with Consideration of Power Limit. *Power Electron.* **2022**, *56*, 86–89.

7. Du, Y.; Yan, M.M.; Wang, X. Dynamic Power Control Strategy for interlinking Converter Under Bilateral inertia Constraints in AC/Dc subgrid. *Autom. Electr. Power Syst.* **2023**, *47*, 172–179.

8. Chen, X.; Zhou, J.; Shi, M.; Yan, L.; Zuo, W.; Wen, J. A Novel Virtual Resistor and Capacitor Droop Control for HESS in Medium Voltage DC System. *IEEE Trans. Power Syst.* **2019**, *34*, 2518–2527. [CrossRef]

9. Bharatee, A.; Ray, P.K.; Ghosh, A. A power management scheme for grid-connected PV integrated with hybrid energy storage system. *J. Mod. Power Syst. Clean Energy* **2022**, *10*, 954–963. [CrossRef]

10. Chen, J.W.; Zhou, J.; Zhang, W.Q. Hybrid Energy Storage Power Allocation Strategy Based on Wavelet Packet-Fuzzy Algorithm. *Smart Power* **2023**, *51*, 61–68.

11. Zhao, Y.X.; Gao, C.P.; Fan, H. Power Coordination Strategy for Hybrid Energy Storage in AC/Dc Microgrids Based on Virtual lmpedance-Fuzzy Algorithm. *J. Shanghai Jiaotong Univ.* **2023**, *1*, 23. [CrossRef]

12. Wang, L.; Hu, J.C.; Zeng, X.J. Hierarchical Coordinated Power Control Strategy for AC-DC Hybrid Microgrid with Hybrid Energy Storage. *Trans. China Electrotech. Soc.* **2024**, *39*, 2311–2324.

13. Li, J.F.; Wang, Y.; Cheng, X.X.; Xiong, X.Z.; Sun, J.K. Configuration Method of Photovoltaic Storage Capacity in Microarid Svstem Based on Bi-Laver Ootimization. *Distrib. Energy* **2024**, *9*, 80–88.

14. Ma, W.Z.; Wang, L.B.; Wang, Y.S.; Wan, R.; Wang, X.; Wang, J. Hybrid energy storage power allocation with adaptive virtual inertia control considering SOC. *Power Syst. Prot. Control.* **2024**, *52*, 83–93. [CrossRef]

15. Xie, B.; Li, P.Y.; Su, Y.R.; Su, J.H.; Liu, T.T. Research on Maximum Power Point Tracking Algorithm of PV Array Under Local Shadow. *Acta Energiae Solaris Sin.* **2023**, *44*, 47–52.

16. Liu, X.Y.; Chen, R.; Bai, S.W. Design and analysis of hybrid energy storage system based on supercapacitor. *Chin. J. Power Sources* **2021**, *45*, 1181–1184.